785. Bond graph-based analysis of energy conversion in vibration-piezoelectricity coupling and its application to a cantilever vibration energy harvester

Chuan Li[1, 2, a], Daewoong Hong[2, b], Kwang-Ho Kwon[2, c], Jaehwa Jeong[2, d]
[1]School of Mechanical Engineering, Chongqing Technology and Business University
Chongqing 400067, P. R. China
[2]Department of Control and Instrumentation Engineering, Korea University
Chungnam 339-700, South Korea
E-mail: [a]*chuanli@21cn.com*, [b]*smiletong@korea.ac.kr*, [c]*kwonkh@korea.ac.kr*, [d] *jaehwa@korea.ac.kr*

(Received 7 February 2012; accepted 14 May 2012)

Abstract. The energy flow in a piezoelectric vibration energy harvester (VEH) involves both the mechanical domain and the electrical domain. To better understand the vibration-piezoelectricity coupling of this device, a unified description approach based on the bond graph is proposed to analyze the influence of the piezoelectric VEH parameters on the electricity harvesting performance in the energy conversion. Both the mechanical structure and the electric circuit are modeled using the bond graph. The present method is applied to analyze the parametric configuration of a piezoelectric VEH, which is further tested on an experimental platform. The results show that the unified model using the bond-graph is well-suited for analyzing the vibration-piezoelectricity coupling. The proposed method can advance the design optimization of piezoelectric VEHs.

Keywords: vibration energy harvesting, bond graph, coupling, cantilever, piezoelectricity.

1. Introduction

Miniaturized wireless electronic systems have been calling for the development of self-powered sources to replace the conventional battery, which often suffers from its large volume and limited lifetime. As environmental vibration is one of the most important energy reservoirs, vibration energy harvesting that converts natural vibration into μW or nW level electrical energy is emerging as one of the promising alternatives to the conventional battery for such systems as wireless sensor networks [1].

To extract electrical energy from surrounding vibration, three transduction mechanisms are used: electrostatic, electromagnetic and piezoelectric [2]. Due to simple structure and higher conversion ratio in terms of mechanical-electrical coupling, the piezoelectric vibration energy harvester (VEH) has been considered as one of the most convenient technologies for renewable power supplies.

Piezoelectric materials can generate an electrical charge when subjected to a mechanical stress or stain, and vice versa. Recently, different kinds of piezoelectric VEHs have been developed to meet the various requirements of real applications [3]. In addition to attention on fabrication, much effort has also directed on performance analyses, the results of which can be used for the design optimization of harvesting devices. Kim et al. [4] designed and analyzed a PZT cantilever for low frequency vibration energy harvesting. Dauksevicius et al. [5] employed the multiphysical FE (finite element) approach to analyze a contact-type piezotransducer for ambient vibration harvesting. Based on the revised impendence matching theory, Liang et al. [6] proposed a methodology for maximum power harvesting. The researches on the VEHs have achieved good results with respect to one or more of the three basic stages: mechanical resonator, piezoelectric transducer and load circuit [7].

Since the energy flow in a piezoelectric VEH involves both the mechanical domain and the electrical domain, one should consider the three basic stages in a unified aspect. Moreover, the mechanical-electrical coupling of the piezoelectric transducer makes it difficult to analyze the

three stages separately. A bond graph is a graphical approach that can model a dynamic system in a wide variety of domains (e.g., electrical, fluid, thermal, magnetic and mechanical domains) [8, 9]. Considering the fact that piezoelectric behavior is related to different fields, Boukari et al. [10] used the bond graph to model piezo-actuators. The piezo-actuators focus heavily on the controllable actuation and the piezoelectric VEH, on the contrary, the harvestable energy. In this paper, based on the individual analysis of the three constituents, the bond graph method is employed to formulate the energy flow in a cantilever VEH. Because energy conversion and energy coupling in different domains are bonded in a unified fashion, energy harvesting performance is evaluated in terms of different parameters. In addition to the theoretical analysis, an experimental setup is also presented to validate the proposed unified analysis approach.

The rest of this paper is accordingly organized as follows. In Section 2 we present the architecture of the cantilever VEH using the bond graph approach. The unified analysis model of the energy coupling is also presented in this section. This unified model is subsequently applied to the parametric analysis of the cantilever VEH in Section 3. Experiments are carried out, and the results are compared with the calculated data in Section 4. Conclusions are given in Section 5.

2. Description of Vibration-Piezoelectricity Coupling Using Bond Graph

A cantilever VEH, even with its very simple structure, can produce a large deformation under vibration, as shown in Fig. 1. To enlarge the beam deformation and reduce the resonance frequency, a proof mass is accordingly attached on the free end of the beam. The cantilever beam covered with a unimorph or a bimorph moves in response to the base vibration. For simplification, the unimorph case is taken as the basic example to illustrate our approach. More complicated cases can also be analyzed by our method. Let three axes of the global coordinates be 1, 2 and 3 respectively. The base displacement $y(t)$ along no. 2 axis leads to the vibration of the proof mass $y(t) + z(t)$ and further causing the electric potential differences $v(t)$ between the two surfaces of the piezoelectric material.

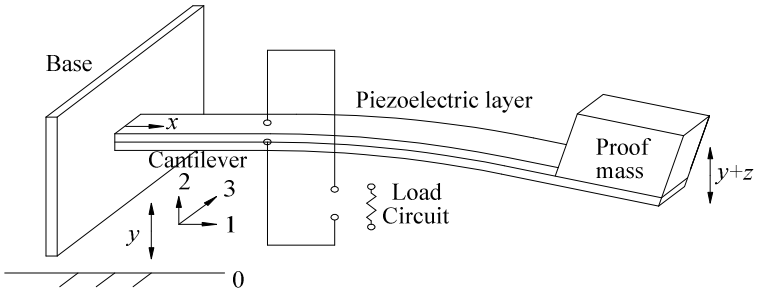

Fig. 1. Schematic diagram of a cantilever VEH

As mentioned in Section 1, the three stages of a VEH respectively play different roles in energy harvesting. The mechanical resonator including a base frame, a cantilever beam and a proof mass produces large vibration energy resulting from the surroundings. The load circuit creates the electrical context needed by the end product. The piezoelectric transducer, therefore, links the vibration energy generation and the electricity consumption.

The first stage (i.e., the mechanical resonator) of the VEH can be represented by a lumped parametric model consisting of a mass (m_m), a damper (d_m) and a spring (s_m) in the mechanical domain. The vibration force (F_m) is then transformed by the piezoelectric transducer (i.e. the second stage of the VEH), which can be modeled as a transformer (TF) with ratio n [11]. The dielectric effect of the piezoelectric layer is regarded as a clamped capacitor (C_p) connected to

the secondary coil of the *TF* in parallel. For real applications, the load is often combined with nonlinear resistance, capacitance and inductance. In this paper, a resistor (R_l) is suggested to denote the load circuit in the electrical domain. It is worth noting that the cantilever also bears the electricity-induced damping force resulting from the piezoelectric transducer and the load circuit, though the fact that the first coil of *TF* is determined mainly by the mechanical vibration. An equivalent damper (d_p) is suggested to denote this electricity-induced damping effect in the mechanical domain. Taking the aforementioned factors into account, we present a bond graph as shown in Fig. 2 to depict the energy flow in the VEH.

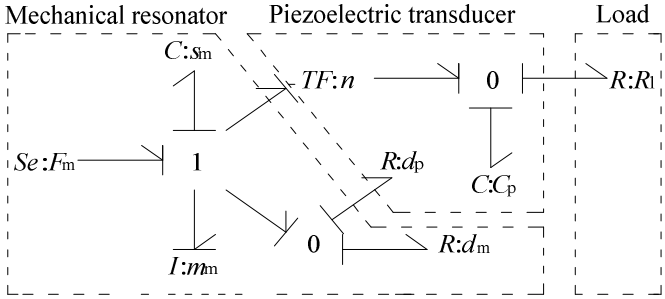

Fig. 2. Bond graph representation of energy harvesting

After determining VEH architecture, as shown in Fig. 2, parameters are formulated in analytical form to illustrate the energy flow. Suppose the absolute displacement of the base under environmental vibration excitation is *y* (see Fig.1), the absolute displacement of the proof mass is *y* + *z*, and the equivalent mass of the VEH at the point of proof mass is *m*. The vibration force acting on the mass consists of the vibration force F_m and the inertial force F_z, i.e.:

$$F = m\ddot{y} + m\ddot{z} = F_m + F_z \tag{1}$$

Let *x* denote the distance from the base, *I* the effective moment of inertia of the beam, l_p the length of the piezoelectric layer, l_m the length of the mass, t_p the thickness of the piezoelectric layer, t_b the thickness of the metal beam, and E_p the Young's modulus of the piezoelectric layer, one can correlate the vibration force with the proof mass vibration displacement as [12]:

$$\frac{\mathrm{d}^2 z}{\mathrm{d}x^2} = \frac{F_m(l_p + l_m/2 - x)}{E_p I} \tag{2}$$

Solving for *z* from the above equation, at the free end of the piezoelectric layer (i.e. $x = l_p$), one has:

$$F_m = \frac{2E_p I}{l_p^2(2l_p/3 + l_m/2)} z \tag{3}$$

On the other hand, the vibration force F_m leads to the stress:

$$\sigma = \frac{1}{l_p}\int_0^{l_p} \frac{t_p F_m(l_p + l_m - x)}{I}\mathrm{d}x \tag{4}$$

The above equation can be rewritten as:

$$\sigma = \frac{(l_p + 2l_m)t_p}{2I} F_m \tag{5}$$

The relation between the stress σ and the strain δ is given by:

$$\sigma = \delta E_p \tag{6}$$

Combining equations (3), (5) and (6) yields:

$$z = \frac{l_p^2(2l_p + 3l_m/2)}{3t_p(l_p + 2l_m)} \delta \tag{7}$$

Let $k_1 = \frac{(l_p + 2l_m)t_p}{2I}$, $k_2 = \frac{l_p^2(2l_p + 3l_m/2)}{3t_p(l_p + 2l_m)}$ and $k_3 = \frac{2E_p I}{l_p^2(2l_p/3 + l_m/2)}$. The equations (3), (5) and (7) can be rewritten as:

$$\left.\begin{aligned} \sigma &= k_1 F_m \\ z &= k_2 \delta \\ F_m &= k_3 z \end{aligned}\right\} \tag{8}$$

The equivalent lumped parameters m_m, d_m and s_m respectively correspond to the second-, first- and zero-order time derivative of the stress. According to equations (1) and (8), one can obtain the stress (σ_m) acting on the equivalent mass m_m as follows:

$$\sigma_m = k_1 m \ddot{z} = k_1 k_2 m \ddot{\delta} \tag{9}$$

Letting d_{mp} stand for the combination of the mechanical domain equivalent damper d_m and the electricity-induced damper d_p, we have [13]:

$$d_{mp} = 2\xi\omega_0 \tag{10}$$

where ξ and ω_0 denote the dimensionless damping ratio and the natural angular frequency, respectively. The stress acting on d_{mp} is given by:

$$\sigma_{mp} = k_2 d_{mp} \dot{\delta} \tag{11}$$

Since the Young's modulus of the metal beam is much greater than that of the piezoelectric material, i.e. $E_b >> E_p$, according to equation (6), we have:

$$\sigma_s = E_s \delta \tag{12}$$

According to equations (3), (8), (9), (11) and (12), the bond graph parameters in the mechanical domain (and d_p in the piezoelectric domain) as shown in Fig. 2 are formulated as:

$$\left.\begin{aligned} F_m &= k_3 z \\ m_m &= k_1^2 k_2 m \\ d_m + d_p &= k_1 k_2 d_{mp} \\ s_m &= k_1 E_s \end{aligned}\right\} \tag{13}$$

In the second stage (piezoelectric transducer), the governing equations for the unimorph are given by [14]:

$$\left.\begin{aligned} \delta &= \sigma_t / E_p + d_{31} H \\ D &= \varepsilon H + d_{31} \sigma_t \end{aligned}\right\} \tag{14}$$

where H represents the electric field, σ_t the strain of the equivalent transformer, d_{31} - the piezoelectric strain coefficient, ε - dielectric constant of the piezoelectric material, and $D = d_{31} E_p \varepsilon$ - electric displacement.

The energy conversion in the piezoelectric layer is analogous to that of a transformer according to the bond graph shown in Fig. 2. The "transformer" *TF* converts the stress to an electric field at zero strain (i.e. $\delta = 0$). According to Equation (14), one has:

$$\sigma_t = -d_{31} E_p H \tag{15}$$

It is well known that the voltage V is the product of the electric field and the distance, i.e.:

$$V = H t_p \tag{16}$$

Substituting equation (16) into equation (15) results in:

$$\sigma_t = \frac{-d_{31} E_p}{t_p} V \tag{17}$$

According to equations (8) and (17), the transformer *TF* in the bond graph as shown in Fig. 2 transforms the strain into voltage with the transformation ratio $n = \dfrac{-k_1 t_p}{d_{31} E_p}$.

Finally, the capacitor of the piezoelectric layer can be formulated using the definition of a capacitor as follows:

$$C_p = \frac{\varepsilon_0 w l_p}{2 t_p} \tag{18}$$

where w represents the width of the piezoelectric layer (metal beam), and ε_0 is vacuum dielectric constant ($\varepsilon_0 = 8.85419 \times 10^{-12} \mathrm{C}^2/\mathrm{J \cdot m}$).

So far, we have formulated all the components in the bond graph except the load resistor R_l. We will further evaluate the load resistor and other performance parameters in the following section.

3. Energy Harvesting Performance Estimation Using the Proposed Bond Graph

Different configurations will result in different energy harvesting performance. The proposed unified bond graph can optimize mechanical, piezoelectric and loading parameters simultaneously. Because resonance frequency, output voltage and output power are three classical performance parameters in real applications, we estimate the three parameters based on the proposed bond graph as follows.

Let ρ_b and ρ_p represent the densities of the metal beam and the piezoelectric layer respectively. Suppose the inertial mass of the proof mass is m_e. The cantilever beam and the proof mass are assumed to be a point mass with an equivalent vertical force at the free end of the beam. This mass m can be expressed as [15]:

$$m = 33(\rho_b + \rho_p) l_p w(t_b + t_p)/140 + m_e \tag{19}$$

The bending modulus per unit width is given by [2]:

$$D_p = \frac{E_p^2 t_p^4 + E_b^2 t_b^4 + 2E_p E_b t_p t_b (2t_p^2 + 2t_b^2 + 3t_p t_b)}{12(E_p t_p + E_b t_b)} \tag{20}$$

This results in the analytical expression of the natural angular frequency:

$$\omega_0 = 1.7069\sqrt{\frac{D_p w}{(l_p + l_m/2)^3 m}} \tag{21}$$

According to the energy flow shown in the proposed bond graph (Fig. 2), we have:

$$\left.\begin{aligned} F_m &= m_m \ddot{\delta} + (d_m + d_p)\dot{\delta} + s_m \delta + nV \\ \dot{V} &= \frac{-d_{31} E_p t_p}{\varepsilon}\dot{\delta} - \frac{V}{R_l C_p} \end{aligned}\right\} \tag{22}$$

Combining equations (1), (13), (17) and (22) in the Laplace's domain yields:

$$\left.\frac{\hat{V}}{\hat{z}}\right|_{R_l} = \frac{-k_3 d_{31} E_p t_p R_l C_p s}{(k_1^2 k_2 m s^2 + k_1 k_2 (d_m + d_p) s + k_1 E_s)(\varepsilon R_l C_p s + \varepsilon) - n k_3 d_{31} E_p t_p R_l C_p s} \tag{23}$$

where ^ denotes the Laplace representation, and s the Laplace calculus. The relation between the output power P and the input vibration displacement z in the Laplace's domain is accordingly given by:

$$\left.\frac{\hat{P}}{\hat{z}^2}\right|_{R_l} = \left(\hat{V}/\hat{z}\Big|_{R_l}\right)^2 \Big/ R_l . \tag{24}$$

Usually, output power maximization is one of the most important objectives in vibration energy harvesting. Suppose there is an optimal resistor R_{lopt} corresponding to the maximum output power. This means that the function $P(R_l)$ is a vertex. Solving the following equation:

$$\frac{\partial\left(\left|\left(\hat{V}/\hat{z}\right|_{R_l}\right)^2 \Big/ R_l\Big|_{s=j\omega}\right)}{\partial R_l} = 0 \tag{25}$$

results in the closed-form of the optimal load resistor:

$$R_{lopt} = \mathrm{mod}\left(\frac{\varepsilon k_1^2 k_2 m s^2 + k_1 k_2 (d_m + d_p)\varepsilon s + \varepsilon k_1 E_s}{C_p(\varepsilon k_1^2 k_2 m s^3 + k_1 k_2 (d_m + d_p)\varepsilon s^2 + \varepsilon k_1 E_s s - n k_3 t_p d_{31} E_p s)}\Big|_{s=j\omega}\right) \tag{26}$$

On the other hand, for the open circuit (i.e. $R_l \to \infty$) condition of the proposed bond graph, equation (22) can be rewritten as:

$$\left.\begin{aligned} F_m &= m_m \ddot{\delta} + (d_m + d_p)\dot{\delta} + s_m \delta + nV \\ V &= \frac{-d_{31} E_p t_p}{\varepsilon}\delta \end{aligned}\right\}, \tag{27}$$

leading to the open circuit voltage, which can be calculated from the following equation:

$$\frac{\hat{V}}{\hat{z}}\Big|_{R_l \to \infty} = \frac{-k_3 d_{31} E_p t_p}{(k_1^2 k_2 m s^2 + k_1 k_2 (d_m + d_p)s + k_1 E_s)\varepsilon + n k_3 d_{31} E_p t_p} \tag{28}$$

4. Experiments and Discussions

In this section, the proposed bond graph and the related parametric estimation model were evaluated by testing a cantilever VEH on an experimental setup. As shown in Fig. 3, a cantilever VEH (fabricated in the Korea University lab) was fixed on a base (manufactured in the Korea University lab), which was directly connected to the output shaft of a vibration exciter (B&K, type 4810). The vibration exciter was driven by a power amplifier (B&K, type 2718), which was controlled by a dynamic signal analyzer (DSA, HP, type 35670A). According to the predefined waveforms of the DSA, the vibration exciter generated the vibration for the VEH. Due to the signal transfer from the DSA, the amplifier to the vibration exciter, signal attenuation was usually unavoidable in the setup. Therefore, an accelerometer (PCB, type 333B52) was mounted on the top of the VEH base to measure the real vibration acceleration, which was input to the DSA via a signal conditioner (PIEZOTRONICS, type 482C). To monitor the real-time voltage signal harvested by the VEH, the output voltage of the VEH was also acquired by the DSA. A built-in 3.5" floppy drive was included in the DSA so that the measured data (both acceleration and voltage simultaneously) could be saved on floppy disks for further use.

The piezoelectric film of the VEH was made from Polyvinylidene Fluoride (PVDF). The geometric and material specifications of the cantilever VEH are illustrated in Table 1.

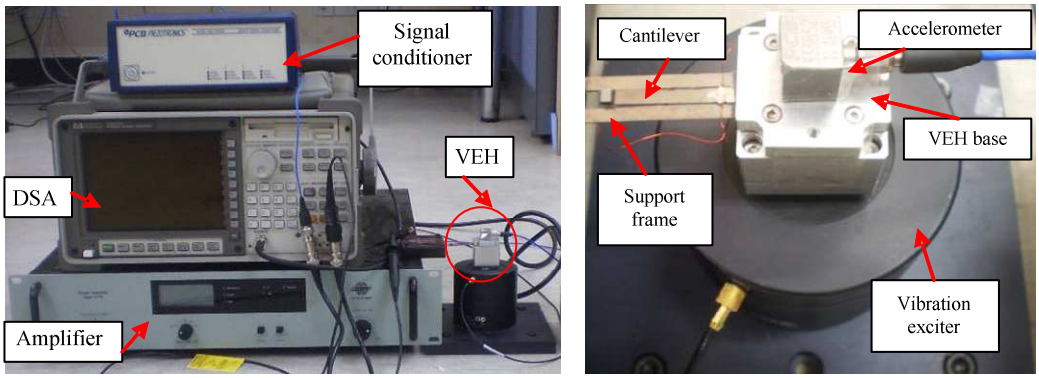

(a) (b)

Fig. 3. Experimental setup: (a) overview and (b) enlarged view of the VEH

Table 1. Geometric and material properties of the cantilever VEH

Nomenclature		Value
L_P	PVDF length	24×10^{-3} m
T_p	PVDF thickness	28×10^{-6} m
Y_p	PVDF Yong's modulus	3×10^{9} Pa
ε	PVDF dielectric constant	$12\times\varepsilon_0$
d_{31}	PVDF strain coefficient	20×10^{-12} V^{-1}
k_{31}	PVDF coupling coefficient	0.12
W	PVDF (beam) width	3×10^{-3} m
T_b	Beam thickness	3×10^{-4} m
ρ_b	Beam density	2.71×10^{3} kg/m^3
Y_b	Beam Yong's modulus	68.5×10^{9} Pa
L_m	Proof mass length	2×10^{-3} m
W_m	Inertial mass of the proof mass	9.0720×10^{-5} kg
ζ	Unitless damping ratio	0.01

We first tested the open circuit voltage estimation performance of the proposed method. A swept harmonics signal was employed as the exciting vibration, i.e., $z(t) = A(t)\sin(f(t)+\varphi)$, where A denotes the amplitude, f the frequency and φ the phase of the signal. Fig. 4a shows the amplitude of the vibration signal collected by the accelerometer. It shows that $A(t)$ varies between 0.8481g to 2.042g (1g = 9.8 m/s^2) and $f(t)$ ranges between 50 Hz to 250 Hz. The corresponding voltage amplitude signal harvested by the VEH is plotted in Fig. 4b. The bond graph–based performance estimation model was also employed to calculate the output voltage amplitude according to equation (28). The calculated data are also shown in Fig. 4b for comparison. The calculated natural frequency was 143.5 Hz. The measured first-mode resonant frequency, for comparison, was 142 Hz, which indicated that the proposed bond graph-based analysis accurately estimated the output voltage and resonant frequency.

The vibration amplitude at the resonant frequency was subsequently fixed at around 1g to measure the output voltage and power for different loads. The measured voltage amplitude and the related maximum output power (at the resonant frequency) are plotted in Fig. 5a and Fig. 5b respectively. For comparison, equations (23) and (24) were employed to generate the estimation data for different load resistors. The calculated results are respectively illustrated in Fig. 5a and Fig. 5b as a dashed line. Using equation (26), the optimal resistance is calculated as R_{lopt} = 2.5312 MΩ.

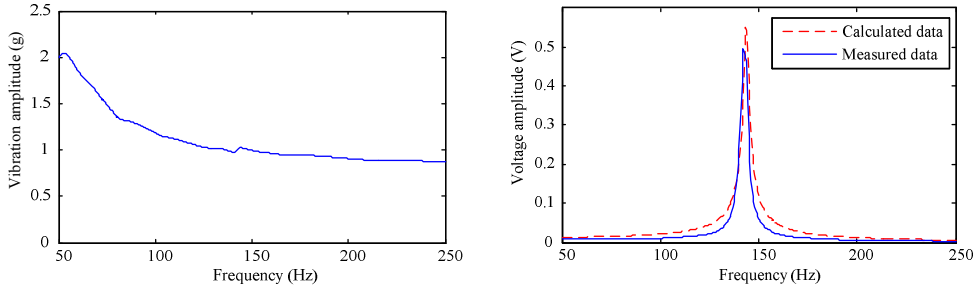

(a) (b)

Fig. 4. Open circuit experiment results:
(a) vibration amplitude and (b) comparison of calculated and measured voltage amplitudes

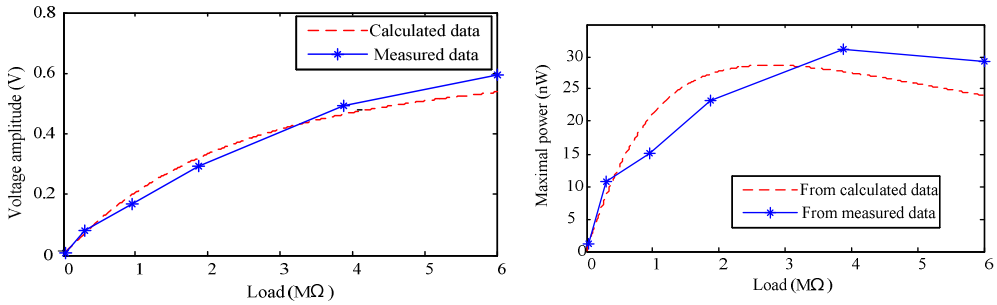

(a) (b)

Fig. 5. Experiment results for different load resistances:
(a) voltage amplitude at resonant frequency and (b) maximum output power at resonant frequency

The comparison of the measured voltage amplitude with the calculated one, as shown in Fig. 5a, indicates that the calculated data were consistent with the measured data. When both data are applied to calculate the maximum power, however, a greater error can be identified from Fig. 5b. This is due to the fact that the power is directly related to the square of the voltage, increasing the error by a square ratio. Nonetheless, the maximum output power at the resonance frequency was 31.08 nW, as calculated from the measured data. On the contrary, the simulation result showed that the maximum output power was 28.68 nW. This further confirmed that the proposed method tracked the output energy trend with a good precision.

Owing to its estimation capability, the proposed method was then applied to analyze the influence of VEH configuration on the electrical output. Letting the amplitude of the input vibration $A(t)$ = 0.8g, Fig. 6a shows the influence of the cantilever width w on the open circuit voltage amplitude calculated according to Section 3 (other parameters are fixed as shown in Table 1). For w = 2.5 mm, 2.8 mm, 3 mm, 3.2 mm and 3.5 mm respectively, the first-mode resonant frequency was 133 Hz, 139.5 Hz, 143.5 Hz, 147.5 Hz and 153 Hz respectively, and the amplitude of the open circuit voltage 0.6568 V, 0.5999 V, 0.5699 V, 0.5350 V and 0.4968 V, respectively.

Once again we applied the proposed model to analyze the influence of the coupling coefficient k_{31} on the maximum output power. Again we let the amplitude of the input vibration $A(t)$ = 0.8g. Fig. 6b plots the change of the maximum output power (at the natural frequency f_0 = 143 Hz for different loads (0~6 MΩ) and coupling coefficients (other parameters were fixed as shown in Table 1). With the increase of k_{31} from 0.10 to 0.15, the maximum output power dropped from 22.69 nW to 14.30 nW in the calculation cases.

Based on the above results, one can observe that both mechanical and electrical parameters have significant influence on the energy harvesting performance. It is noted that only the

representative calculations are provided in this section. Since more parametric influences can be calculated using the above method, the proposed method can be employed to obtain the expected energy harvesting performance for different VEH configurations.

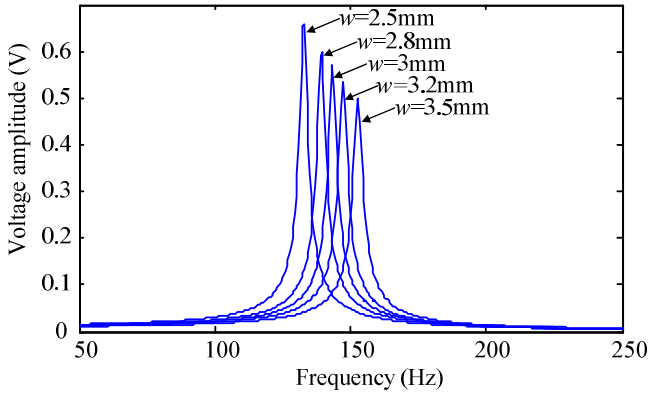

(a)

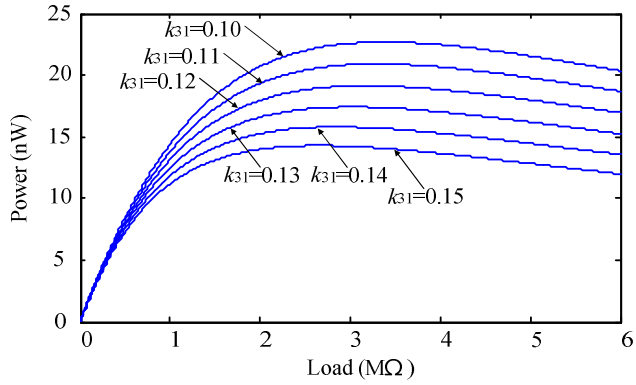

(b)

Fig. 5. Experimental results for different load resistances:
(a) voltage amplitude at resonant frequency, and (b) output power at resonant frequency

5. Conclusions

A graph-based approach was proposed to analyze the energy flow and energy conversion of piezoelectric vibration energy harvesters. The top-down architecture was used for the bond graph modeling. The VEH was regarded as an entity with three stages in terms of energy domain: mechanical domain, electrical domain or mechanical-piezoelectric coupling. In each stage, different dynamical characteristics were represented as graphic components using a unified fashion. Considering the vibration-piezoelectricity coupling, we formulated the components of the bond graph based on the conservation of energy. As an effective tool for understanding multi-domain systems, the proposed bond graph-based model dealt with the energy conversion of the VEH in a unified fashion.

The proposed unified analysis approach was employed to estimate energy harvesting performance. Natural frequency, output voltage and power were simulated using the bond graph model. A cantilever VEH was fabricated and tested on an experimental setup. The comparison

of the measured data with the calculation results confirmed the effectiveness of the proposed method.

Acknowledgements

This work is supported in part by the Mid-Career Researcher Program through an NRF grant funded by the MEST (No. 2009-0085863) of the Korean Government, the National Natural Science Foundation of China (50905193, 51035008) and the Natural Science Foundation Project of CQ CSTC (2010BB4261).

References

[1] **Kim H. S., Kim J. H., Kim J.** A review of piezoelectric energy harvesting based on vibration. International Journal of Precision Engineering and Manufacturing, Vol. 12, Issue 6, 2011, p. 1129-1141.

[2] **Beedy S. P., Tudor M. J., White N. M.** Energy harvesting vibration sources for microsystems applications. Measurement Science and Technology, Vol. 17, Issue 12, 2006, p. R175-R195.

[3] **Reilly E. K., Burghardt F., Fain R., Wright P.** Powering a wireless sensor node with a vibration-driven piezoelectric energy harvester. Smart Materials and Structures, Vol. 20, Issue 12, 2011, 125006 (8 p.).

[4] **Kim M., Hwang B., Min N. K., Jeong J. H., Kwon K. H., Park K. B.** Design and fabrication of a PZT cantilever for low frequency vibration energy harvesting. Journal of Nanoscience and Nanotechnology, Vol. 11, Issue 7, 2011, p. 6510-6513.

[5] **Dauksevicius R., Kulvietis G., Ostasevicius V., Gaidys R., Milasauskaite I.** Multiphysical modeling of a contact-type piezotransducer for the analysis of micro-energy harvesting from ambient vibrations. Journal of Vibroengineering, Vol. 13, Issue 2, 2011, p. 342-351.

[6] **Liang J., Liao W. H.** Impedance modeling and analysis for piezoelectric energy harvesting systems. IEEE/ASME Transactions on Mechatronics, 2012, doi: 10.1109/ TMECH, 2011, 2160275.

[7] **Galayko D., Basset P.** A general analytical tool for the design of vibration energy harvesters (VEHs) based on the mechanical impedance concept. IEEE Transactions on Circuit and Systems – I: Regular Papers, Vol. 58, Issue 2, 2011, p. 299-311.

[8] **Gawthrop P. J., Bavan G. P.** Bond graph modeling. IEEE Control System Magazine, Vol. 27, Issue 2, 2007, p. 24-45.

[9] **Xing Y. H., Pedersen E., Moan T.** An inertia-capacitance beam substructure formulation based on the bond graph method with application to rotating beams. Journal of Sound and Vibration, Vol. 330, Issue 21, 2011, p. 5114-5130.

[10] **Boukari A. F., Carmona J. C., Moraru G., Malburet F., Chaaba A., Douimi M.** Piezo-actuators modeling for smart applications. Mechatronics, Vol. 21, Issue 1, 2011, p. 339-349.

[11] **Flynn A. M., Sanders S. R.** Fundamental limits on energy transfer and circuit considerations for piezoelectric transformers. IEEE Transactions on Power Electronics, Vol. 17, Issue 1, 2002, p. 8-14.

[12] **Ajitsaria J., Choe S. Y., Shen D., Kim D. J.** Modeling and analysis of a bimorph piezoelectric cantilever beam for voltage generation. Smart Materials and Structures, Vol. 16, Issue 2, 2007, p. 447-454.

[13] **Roundy S. J.** Energy Scavenging for Wireless Sensor Nodes with a Focus on Vibration to Electricity Conversion. Ph. D. Dissertation, 2003.

[14] **Erturk A., Inman D. J.** A distributed parameter electromechanical model for cantilever piezoelectric energy harvesters. ASME Journal of Vibration and Acoustics, Vol. 130, Issue 4, 2008, 041002 (15 p.).

[15] **Ng T. H., Liao W. H.** Sensitivity analysis and energy harvesting for a self-powered piezoelectric sensor. Journal of Intelligent Material Systems and Structures, Vol. 16, Issue 10, 2005, p. 85-97.